The critical current density of an SNS Josephson-junction in high magnetic fields

2013 Supercond. Sci. Technol. 26 065007

(http://iopscience.iop.org/0953-2048/26/6/065007)

Supercond. Sci. Technol. **26** (2013) 065007 (9pp) doi:10.1088/0953-2048/26/6/065007

The critical current density of an SNS Josephson-junction in high magnetic fields

George J Carty and Damian P Hampshire

Department of Physics, Superconductivity Group, Centre for Materials Physics, University of Durham, South Road, Durham DH1 3LE, UK

E-mail: d.p.hampshire@durham.ac.uk

Received 25 February 2013, in final form 26 February 2013
Published 30 April 2013
Online at stacks.iop.org/SUST/26/065007

Abstract
Although the functional form of the critical current density (J_c) of superconducting–normal–superconducting (SNS) Josephson-junctions (J-Js) has long been known in the very low field limit (e.g. the sinc function), includes the local properties of the junction and has been confirmed experimentally in many systems, there have been no such general solutions available for high fields. Here, we derive general analytic equations for J_c in zero field and in high fields across SNS J-Js for arbitrary resistivity of the superconductor and the normal layer which are consistent with the literature results available in limiting cases. We confirm the validity of the approach using both computational solutions to time-dependent Ginzburg–Landau (TDGL) theory applied to SNS junctions and experimental J_c data for an SNS PbBi–Cd–PbBi junction. We suggest that since SNS junctions can be considered the basic building blocks for the description of the grain boundaries of polycrystalline materials because they both provide flux-flow channels, this work may provide a mathematical framework for high J_c technological polycrystalline superconductors in high magnetic fields.

1. Introduction

Some aspects of the research into the properties of superconductors in magnetic fields are rather compartmentalized. Research on Josephson-junctions (J-Js) in low fields, be that for high-speed computers or voltage standards [1], concentrates on studying the local structural and electronic properties of grain boundaries (or normal layers) on very small length scales because they strongly affect technological performance [2, 3]. On the other hand, research considering the critical current density (J_c) of high field polycrystalline superconductors, used for applications from MRI scanners and particle accelerators to fusion tokamaks [4], is generally parameterized using scaling laws which usually do not include local grain boundary properties at all. At criticality, fluxons depin [5] from isolated pinning sites or free fluxons shear past pinned fluxons as part of the flux line lattice [6] and flux flow consists of a series of separate pinning site events. We attribute this compartmentalization predominantly to the lack of a mathematical framework that can describe how the local properties of grain boundaries affect J_c in high magnetic fields. Such a framework is required to synthesize our understanding of the effects of local grain boundary properties on J_c with our understanding of the many fluxons and pinning sites that must be considered in high fields and will help bring the research on J-Js to bear on understanding and improving polycrystalline superconductors for high field applications. In this paper, we analyse the current density through superconducting–normal–superconducting (SNS) junctions because we suggest they can provide useful building blocks for describing grain boundaries in polycrystalline superconductors. We derive general analytic expressions for J_c across SNS J-Js in zero field and in high magnetic fields for superconductors and normal layers with arbitrary resistivity, which are consistent with limiting-case solutions available in the literature. These expressions allow one to relate high field critical current density measurements to the properties of the normal layer. We confirm the solutions obtained by comparison with computational solutions using time-dependent Ginzburg–Landau (TDGL) theory and with

experimental in-field variable-temperature J_c data on a PbBi–Cd–PbBi SNS junction. Finally, we discuss future work, which will include using the functional form proposed to describe J_c in polycrystalline materials.

2. Time-dependent Ginzburg–Landau theory

The Ginzburg–Landau theory of superconductivity [7] follows from the Landau theory of second-order phase transitions, but uses a complex order parameter ψ such that $|\psi|^2$ equals the density of superconducting electrons. It provides a way of describing superconductivity that is more complete than simple macroscopic models [8] but without the extreme complexity of microscopic theory that makes calculations of the mixed state for example, impractical. The theory has been extended to include time-dependent behaviour where in standard form the TDGL equations are [9, 10].

$$\frac{1}{\xi_{(S)}^2}\left(|\hat{\psi}_{(S)}|^2-1\right)\hat{\psi}_{(S)}+\left(\frac{\nabla}{\mathrm{i}}-\frac{2e}{\hbar}\mathbf{A}\right)^2\hat{\psi}_{(S)} + \gamma'\left(\frac{\partial}{\partial t}+\mathrm{i}\frac{2e}{\hbar}\varphi\right)\hat{\psi}_{(S)}=0 \tag{1}$$

and

$$\mathbf{J}=\frac{\hbar}{2e\mu_0\lambda_{(S)}^2}\mathrm{Re}\left(\hat{\psi}_{(S)}^*\left(\frac{\nabla}{\mathrm{i}}-\frac{2e}{\hbar}\mathbf{A}\right)\hat{\psi}_{(S)}\right) - \frac{1}{\rho_{(S)}}\left(\nabla\varphi+\frac{\partial\mathbf{A}}{\partial t}\right) \tag{2}$$

where the normalized wavefunction $\hat{\psi}_{(S)}=\psi_{(S)}/\psi_{s0}$ and $\psi_{s0}=|\alpha_s|/\beta_s$. α_s and β_s are the standard Ginzburg–Landau constants, the values of $\xi_{(S)}$ and $\lambda_{(S)}$ are the characteristic lengths for the order parameter and supercurrent respectively, the Ginzburg–Landau parameter $\kappa=\lambda_{(S)}/\xi_{(S)}$ and γ' is usually taken as the inverse normal state diffusivity [10]. These TDGL equations also apply for composite materials (i.e. material 1 and 2) as long as the temperature dependences of the material properties are explicitly included. In the dirty limit [11], microscopic theory gives $\xi=(\pi\hbar D/8k_B(T_c-T))^{\frac{1}{2}}$ and $\lambda=(7\hbar\rho\zeta(3)/4\pi^3\mu_0k_B(T_c-T))^{\frac{1}{2}}$ where T_c is critical temperature, $D=v_F^2\tau/3$ is diffusivity, ρ is the normal state resistivity and $\zeta(3)\approx 1.202$ is the Riemann zeta function. The mathematical description of composite superconductors can then be completed using Usadel theory [12, 13] which gives the following boundary conditions at the interface between the superconductor and the normal barrier [14]:

$$\left[\hat{\psi}_{(S)}\right]_{\text{Interface}}=\left[\hat{\psi}_{(N)}\right]_{\text{Interface}} \tag{3}$$

and

$$\left[\frac{\hat{\mathbf{n}}}{\rho_{(S)}}\cdot\left(\nabla-\frac{2\mathrm{i}e}{\hbar}\mathbf{A}\right)\hat{\psi}_{(S)}\right]_{\text{Interface}} = \left[\frac{\hat{\mathbf{n}}}{\rho_{(N)}}\cdot\left(\nabla-\frac{2\mathrm{i}e}{\hbar}\mathbf{A}\right)\hat{\psi}_{(N)}\right]_{\text{Interface}}. \tag{4}$$

The first boundary condition corresponds to continuity of pair conservation amplitude, while the second corresponds to supercurrent conservation (consistent with equation (2)). We note that the terms 'dirty' and 'clean' can be used to describe the ratio $\rho_{(S)}/\rho_{(N)}$ in appropriate limits, but we avoid that terminology in this paper to avoid confusion with the well-known dirty and clean limits in the general theory of superconductivity [15].

3. One-dimensional analytic solutions for j_c in SNS Josephson-junctions

3.1. General considerations

We can consider current flowing through a one-dimensional SNS Josephson-junction with a normal barrier of thickness $2d$ in the x-direction. With the applied field along the z-axis, the magnetic vector potential $\mathbf{A}$ can be defined as $\mathbf{A}=Bx\hat{y}$ and it is assumed that the normalized order parameter $\hat{\psi}$ depends only on x. Inside the normal junction, equations (1) and (2) are rewritten in 1D:

$$\frac{\hat{\beta}\hat{m}}{\xi_{(S)}^2}\left(|\hat{\psi}_{(N)}|^2+\frac{\hat{\alpha}}{\hat{\beta}}\right)\hat{\psi}_{(N)}-\frac{\mathrm{d}^2\hat{\psi}_{(N)}}{\mathrm{d}x^2} + \left(\frac{2eBx}{\hbar}\right)^2\hat{\psi}_{(N)}=0 \tag{5}$$

$$J=-\frac{\rho_{(S)}}{\rho_{(N)}}\frac{\hbar}{2e\mu_0\lambda_{(S)}^2}\mathrm{Im}\left(\hat{\psi}^*{}_{(N)}\frac{\mathrm{d}\hat{\psi}_{(N)}}{\mathrm{d}x}\right) \tag{6}$$

where $\hat{\alpha}=|\alpha_N/\alpha_S|$, $\hat{\beta}=\beta_N/\beta_S$, $\hat{m}=m_N/m_S$ and $\hat{\psi}_{(N)}=\psi_{(N)}/\psi_{s0}$. Outside the junction, the order parameter is given by [16]:

$$\hat{\psi}_{(S)}(x>d) = \hat{\psi}_\infty\tanh\left(\frac{x_1+x-d}{\xi_{(S)}\sqrt{2}}\right)\exp\left(-\frac{\mathrm{i}\bar{\varphi}}{2}\right) \tag{7}$$

$$\hat{\psi}_{(S)}(x<-d) = \hat{\psi}_\infty\tanh\left(\frac{x_2-x-d}{\xi_{(S)}\sqrt{2}}\right)\exp\left(\frac{\mathrm{i}\bar{\varphi}}{2}\right) \tag{8}$$

where x_1 and x_2 are constants, $\hat{\psi}_\infty$ is the order parameter far from the junction and the phase difference across the junction is $\bar{\varphi}$. In the Meissner state $\hat{\psi}_\infty=1$, and in the mixed state it can be approximated as $\sqrt{1-\frac{B}{B_{c2}}}$.

From these expressions and the boundary conditions one can relate $\hat{\psi}_{(N)}(\pm d)$ and $\frac{\mathrm{d}\hat{\psi}_{(N)}}{\mathrm{d}x}(\pm d)$ to $\hat{\psi}_\infty$ and $\bar{\varphi}$:

$$\frac{\mathrm{d}\hat{\psi}_{(N)}}{\mathrm{d}x}(d)=\frac{\rho_{(N)}}{\xi_{(S)}\rho_{(S)}\sqrt{2}}\left(\hat{\psi}_\infty\exp\left(-\frac{\mathrm{i}\varphi}{2}\right) - \frac{\hat{\psi}_{(N)}^2(d)}{\hat{\psi}_\infty}\exp\left(+\frac{\mathrm{i}\bar{\varphi}}{2}\right)\right) \tag{9}$$

where the general solution for $\hat{\psi}_{(N)}$ is of the form [16]

$$\hat{\psi}_{(N)}(x)=c_1f_1(x)+\mathrm{i}c_2f_2(x). \tag{10}$$

The choice of phases in equations (7) and (8) and the symmetry of the junction ensure f_1 and f_2 are symmetric and

antisymmetric functions respectively, while c_1 and c_2 are real constants. Finding analytic solutions for the current reduces to solving for $\hat{\psi}_{(N)}$ and then substituting into (6). We describe the pair-breaking within the junction by means of a decay length in the normal metal, $\xi_{(DN)}$, defined as

$$\xi_{(DN)} = i\xi_{(S)}\sqrt{\frac{1}{\hat{\alpha}\hat{m}}}. \tag{11}$$

We define $\xi_{(DN)}$ to be an imaginary quantity so that the equations have the same form in both the superconductor and the normal metal, contrary to the usual convention [16, 17] in which $\xi_{(DN)}$ is real. Solutions for $\hat{\psi}_{(N)}$ are derived below where each of the terms $\frac{\hat{\alpha}\hat{m}}{\xi^2_{(S)}}$, $\frac{\hat{\beta}\hat{m}|\hat{\psi}_{(N)}|^2}{\xi^2_{(S)}}$ and $(\frac{2eBx}{\hbar})^2$ in equation (5) are large in turn.

3.2. Zero field J_c—linear equations ($\hat{\alpha}/\hat{\beta} > 0$)

For strong pair-breaking (for example if T is relatively high) then $|\hat{\psi}_{(N)}|^2 \ll 1$ within the junction. The nonlinear term $|\hat{\psi}_{(N)}|^2$ can be ignored and a simple analytic solution is possible [2, 16]. In zero field, the field term can also be ignored so equation (5) can be simplified to [2]

$$\frac{d^2\hat{\psi}_{(N)}}{dx^2} + \frac{\hat{\psi}_{(N)}}{\xi^2_{(DN)}} = 0 \tag{12}$$

which has the well-known solutions [2, 16]

$$f_1 = \cosh\left(\frac{x}{|\xi_{(DN)}|}\right), \qquad f_2 = \sinh\left(\frac{x}{|\xi_{(DN)}|}\right). \tag{13}$$

In the thick junction limit of $\frac{d}{|\xi_{(DN)}|} \gg 1$ we can approximate both f_1 and f_2 so that

$$f_1(d) \approx f_2(d) \approx \frac{1}{2}\exp\left(\frac{d}{|\xi_{(DN)}|}\right) \tag{14}$$

which gives the relationship between $\hat{\psi}_{(N)}$ and its derivative at $x = d$:

$$\frac{d\hat{\psi}_{(N)}}{dx}(d) = \frac{\hat{\psi}_{(N)}(d)}{|\xi_{(DN)}|}. \tag{15}$$

Substituting into (9) and solving for $\hat{\psi}_{(N)}(d)$ gives

$$\left(\frac{\hat{\psi}_{(N)}(d)}{\hat{\psi}_\infty}\exp\left(\frac{i\bar{\varphi}}{2}\right)\right)^2 + \frac{\xi_{(S)}\rho_{(S)}\sqrt{2}}{|\xi_{(DN)}|\rho_{(N)}}\left(\frac{\hat{\psi}_{(N)}(d)}{\hat{\psi}_\infty}\exp\left(\frac{i\bar{\varphi}}{2}\right)\right) - 1 = 0. \tag{16}$$

Solving this quadratic gives:

$$\hat{\psi}_{(N)}(d) = \hat{\psi}_\infty\left[\sqrt{\left(\frac{\xi_{(S)}\rho_{(S)}}{|\xi_{(DN)}|\rho_{(N)}\sqrt{2}}\right)^2 + 1} - \left(\frac{\xi_{(S)}\rho_{(S)}}{|\xi_{(DN)}|\rho_{(N)}\sqrt{2}}\right)\right]\exp\left(-\frac{i\bar{\varphi}}{2}\right). \tag{17}$$

Equating the real and imaginary parts of $\hat{\psi}_{(N)}(d)$ from (17) to those from (10) and (14) gives:

$$c_1 = \hat{\psi}_\infty\left[\sqrt{\left(\frac{\xi_{(S)}\rho_{(S)}}{|\xi_{(DN)}|\rho_{(N)}\sqrt{2}}\right)^2 + 1} - \left(\frac{\xi_{(S)}\rho_{(S)}}{|\xi_{(DN)}|\rho_{(N)}\sqrt{2}}\right)\right]\exp\left(-\frac{d}{|\xi_{(DN)}|}\right)\cos\left(\frac{\bar{\varphi}}{2}\right) \tag{18}$$

$$c_2 = -\hat{\psi}_\infty\left[\sqrt{\left(\frac{\xi_{(S)}\rho_{(S)}}{|\xi_{(DN)}|\rho_{(N)}\sqrt{2}}\right)^2 + 1} - \left(\frac{\xi_{(S)}\rho_{(S)}}{|\xi_{(DN)}|\rho_{(N)}\sqrt{2}}\right)\right]\exp\left(-\frac{d}{|\xi_{(DN)}|}\right)\sin\left(\frac{\bar{\varphi}}{2}\right). \tag{19}$$

We can substitute into (6) to get the maximum critical current J_{D-J} (corresponding to $\bar{\varphi} = \pi/2$) which generalizes the famous (exponential) thickness dependence found by De Gennes [2] to include the $\rho_{(S)}/\rho_{(N)}$ dependence, where:

$$J_{D-J} = \frac{\rho_{(S)}}{\rho_{(N)}}\frac{\hbar\hat{\psi}^2_\infty}{e\mu_0\lambda^2_{(S)}|\xi_{(DN)}|} \times \left\{\sqrt{\left(\frac{\xi_{(S)}\rho_{(S)}}{\sqrt{2}|\xi_{(DN)}|\rho_{(N)}}\right)^2 + 1} - \frac{\xi_{(S)}\rho_{(S)}}{\sqrt{2}|\xi_{(DN)}|\rho_{(N)}}\right\}^2 \times \exp\left(-\frac{2d}{|\xi_{(DN)}|}\right). \tag{20}$$

We denote this (depairing) current density of the junction as J_{D-J} since it is an intrinsic property of the junction comparable to the depairing current for a superconductor.

3.3. Zero field J_c—nonlinear equations ($\hat{\alpha}/\hat{\beta} = 0$)

In an SNS Josephson-junction where $T = T_{c(N)} = 0$, the $\hat{\alpha_N}$ term is zero within the junction, and in zero field the nonlinear term $|\hat{\psi}|^2$ determines the behaviour of the junction. Equation (5) becomes:

$$\hat{\beta}\hat{m}|\hat{\psi}_{(N)}|^2\hat{\psi}_{(N)} = \xi^2_{(S)}\frac{d^2\hat{\psi}_{(N)}}{dx^2}. \tag{21}$$

As before we set $\hat{\psi}(-x) = \hat{\psi}^*(x)$ using (7) and (8). Note that as the first Ginzburg–Landau equation is now nonlinear, f_1 and f_2 are themselves dependent on c_1 and c_2. It is extremely difficult to solve the nonlinear Ginzburg–Landau expression exactly, so we use an approximate solution. One particular solution of (21) is

$$\hat{\psi}_{x_0} = \xi_{(S)}\sqrt{\frac{2}{\hat{\beta}\hat{m}}}\frac{\exp(i\varphi)}{x_0 \pm x} \tag{22}$$

where φ and x_0 are arbitrary real constants. However, this function does not have the required symmetry. This exact solution does however suggest that a trial solution should decay as $1/x$ inside the normal junction, with the function reaching a singularity were it to be extrapolated into the superconductor. Since the function $y = \sec x$ is an even function with singularities at $x = \pm\pi/2$ and the singularities in the extrapolation of ψ are at $\pm x_\infty$ ($x_\infty > d$), we suggest f_1 can be approximated by

$$f_1 = \sec\left(\frac{\pi x}{2x_\infty}\right). \tag{23}$$

We add the requirement that the flow of current through the junction, and therefore $\mathrm{Im}(\hat{\psi}^* \frac{\partial \hat{\psi}}{\partial x})$, must be independent of x. Note that the functions in (13) which lead to the De Gennes result automatically meet this requirement. For f_1 given as (23), f_2 is given by

$$f_2 = \sin\left(\frac{\pi x}{2x_\infty}\right) + \frac{\pi x}{2x_\infty}\sec\left(\frac{\pi x}{2x_\infty}\right). \tag{24}$$

Next c_1 and c_2 are found. Solving the real part and then the phase of (21) at $x = x_\infty$ gives

$$c_1^2 + c_2^2\left(\frac{\pi}{2}\right)^2 = \frac{1}{2\hat{\beta}\hat{m}}\left(\frac{\pi\xi_{(\mathrm{S})}}{x_\infty}\right)^2 \tag{25}$$

and

$$c_2 = -\frac{2c_1}{\pi}\tan\left(\frac{\bar{\varphi}}{2}\right). \tag{26}$$

From these simultaneous equations for c_1 and c_2, we find:

$$c_1 = \frac{\pi\xi_{(\mathrm{S})}}{x_\infty}\sqrt{\frac{1}{2\hat{\beta}\hat{m}}}\cos\left(\frac{\bar{\varphi}}{2}\right) \tag{27}$$

and

$$c_2 = -\frac{2\xi_{(\mathrm{S})}}{x_\infty}\sqrt{\frac{1}{2\hat{\beta}\hat{m}}}\sin\left(\frac{\bar{\varphi}}{2}\right). \tag{28}$$

Substituting into (6) at $x = 0$ gives the current density of J as a function of x_∞:

$$J = \frac{\rho_{(\mathrm{S})}}{\rho_{(\mathrm{N})}}\frac{1}{\hat{\beta}\hat{m}}\frac{\hbar\pi^2}{4e\mu_0\kappa^2 x_\infty^3}\sin\bar{\varphi}. \tag{29}$$

To complete the calculation, we find x_∞ as a function of the junction half-thickness d. In the thick junction limit ($d \approx x_\infty$) we can use the following approximations $\sec(\frac{\pi d}{2x_\infty}) \approx \tan(\frac{\pi d}{2x_\infty}) \approx \frac{2}{\pi}(\frac{1}{1-d/x_\infty})$ to obtain $\hat{\psi}_{(\mathrm{N})}(d)$ and $\frac{\mathrm{d}\hat{\psi}_{(\mathrm{N})}}{\mathrm{d}x}(d)$,

$$\hat{\psi}_{(\mathrm{N})}(d) = \frac{\xi_{(\mathrm{S})}}{x_\infty - d}\sqrt{\frac{2}{\hat{\beta}\hat{m}}}\exp\left(-\frac{\mathrm{i}\bar{\varphi}}{2}\right) \tag{30}$$

$$\frac{\mathrm{d}\hat{\psi}_{(\mathrm{N})}}{\mathrm{d}x}(d) = \frac{\hat{\psi}_{(\mathrm{N})}(d)}{x_\infty - d}. \tag{31}$$

Using (9) gives the value of x_∞:

$$x_\infty = d + \frac{\xi_{(\mathrm{S})}}{\hat{\psi}_\infty}\sqrt{\frac{2}{\hat{\beta}\hat{m}}\left(1 + \frac{\hat{\psi}_\infty\rho_{(\mathrm{S})}}{\rho_{(\mathrm{N})}}\sqrt{\hat{\beta}\hat{m}}\right)}. \tag{32}$$

Substituting into (29), we find the result:

$$J_{\mathrm{D-J}} = \frac{\rho_{(\mathrm{S})}}{\rho_{(\mathrm{N})}}\frac{1}{\hat{\beta}\hat{m}} \times \frac{\hbar\pi^2}{4e\mu_0\kappa^2\left(d + \frac{\xi_{(\mathrm{S})}}{\hat{\psi}_\infty}\sqrt{\frac{2}{\hat{\beta}\hat{m}}\left(1 + \frac{\hat{\psi}_\infty\rho_{(\mathrm{S})}}{\rho_{(N)}}\sqrt{\hat{\beta}\hat{m}}\right)}\right)^3}. \tag{33}$$

3.4. High field J_c in SNS junctions

When $\frac{\hat{\alpha}\hat{m}}{\xi^2_{(\mathrm{S})}}$ and $\frac{\hat{\beta}\hat{m}|\hat{\psi}|^2}{\xi^2_{(\mathrm{S})}}$ are negligible, it is possible to obtain general solutions f_1 and f_2, for equation (5) of the form [16]:

$$f_1(x) = \exp\left(-\frac{eB}{\hbar}x^2\right){}_1F_1\left(\frac{1}{4} - \frac{\hbar}{8eB|\xi_{(\mathrm{DN})}|^2}, 1/2, \frac{2eB}{\hbar}x^2\right) \tag{34}$$

and

$$f_2(x) = x\exp\left(-\frac{eB}{\hbar}x^2\right) \times {}_1F_1\left(\frac{3}{4} - \frac{\hbar}{8eB|\xi_{(\mathrm{DN})}|^2}, 3/2, \frac{2eB}{\hbar}x^2\right) \tag{35}$$

in which ${}_1F_1$ is Kummer's confluent hypergeometric function. For $x \gg \sqrt{\frac{\hbar}{2eB}}$ and $B \gg \frac{\hbar}{8e|\xi_{(\mathrm{DN})}|^2}$ (which will be strictly true at the S–N interfaces of a thick junction in high field), f_1 and f_2 can be approximated by:

$$f_1(x) \approx \frac{\Gamma(1/2)}{\Gamma(1/4)}\left(\frac{\hbar}{2eB}\right)^{1/4}\left(\frac{1}{x^2+\alpha_0^2}\right)^{1/4} \times \exp\left(\frac{eB\gamma}{\hbar}x^2\right) \tag{36}$$

$$f_2(x) \approx \mathrm{sgn}(x)\frac{\Gamma(3/2)}{\Gamma(3/4)}\left(\frac{\hbar}{2eB}\right)^{1/4}\left(\frac{1}{x^2+\alpha_0^2}\right)^{1/4} \times \exp\left(\frac{eB\gamma}{\hbar}x^2\right) \tag{37}$$

where α_0^2 is taken to be zero and γ to be unity. It is important to extend these solutions to lower fields, since in the superconducting state $B/B_{\mathrm{c2}} \leq 1$. Hence we have added α_0^2 and γ so that f_1 and f_2 do not become non-physically large when $\frac{eBd^2}{\hbar}$ is small. Equations (36) and (37) retain $\frac{\mathrm{d}^2\hat{\psi}_{(\mathrm{N})}}{\mathrm{d}x^2} = (\frac{2eBx}{\hbar})^2\hat{\psi}_{(\mathrm{N})}$ when $\alpha_0^2 = \frac{\hbar}{4eB\gamma}$ and $\gamma = 1$ for large x and $\gamma = 1/\sqrt{6} \approx 0.4$ for small x. We have set $\gamma^2 = (1 + eBd^2/\hbar)(6 + eBd^2/\hbar)$ to parameterize the weak field dependence of γ and ensure physically reasonable B-field and x dependences in lower fields while retaining high field accuracy.

Although high field solutions for SNS J-Js are available [16, 18], they are of limited use because they do not include for example general expressions for $\rho_{(S)}/\rho_{(N)}$. This is particularly problematic if we try to generalize work on SNS junctions to address polycrystalline materials since grain boundaries are usually more resistive than intragranular material. Using the method outlined above for solving the linear equations in zero field, we obtain a general in-field solution applicable for all $\rho_{(S)}/\rho_{(N)}$ values. Using (36) and (37) in (9) and (10) to solve for c_1 and c_2 gives:

$$c_1 = \frac{\Gamma(1/4)}{\Gamma(1/2)}\left(\frac{2eB}{\hbar}\right)^{1/4}(d^2+\alpha_0^2)^{1/4}\hat{\psi}_\infty F \times \exp\left(-\frac{eB\gamma d^2}{\hbar}\right)\cos\frac{\bar{\varphi}}{2} \quad (38)$$

where

$$F = \left[\sqrt{\left(\frac{\rho_{(S)}}{\sqrt{2}\rho_{(N)}}\frac{B\gamma}{B_{c2}}\frac{d}{\xi_{(S)}}\left(1-\frac{1}{\frac{2B\gamma}{B_{c2}}\frac{d^2}{\xi_{(S)}^2}+1}\right)\right)^2+1} - \frac{\rho_{(S)}}{\sqrt{2}\rho_{(N)}}\frac{B\gamma}{B_{c2}}\frac{d}{\xi_{(S)}}\left(1-\frac{1}{\frac{2B\gamma}{B_{c2}}\frac{d^2}{\xi_{(S)}^2}+1}\right)\right] \quad (39)$$

and

$$c_2 = \frac{\Gamma(3/4)}{\Gamma(3/2)}\left(\frac{2eB}{\hbar}\right)^{1/4}(d^2+\alpha_0^2)^{1/4}\hat{\psi}_\infty F \times \exp\left(-\frac{eB\gamma d^2}{\hbar}\right)\sin\frac{\bar{\varphi}}{2}. \quad (40)$$

Note the form of $\frac{B\gamma}{B_{c2}}\frac{d^2}{\xi_{(S)}^2}$ is used for convenience and does not depend on the superconducting properties since it is equal to $\frac{eB\gamma d^2}{\hbar}$. Using $\frac{\Gamma(3/4)\Gamma(1/4)}{\Gamma(3/2)\Gamma(1/2)} = 2\sqrt{2}$ and the property of f_1 and f_2 namely: $f_1(x)f_2'(x) - f_1'(x)f_2(x) = \sqrt{\frac{2eB}{\hbar}}$ [16], which ensures that the current density is constant across the junction, we find J_{D-J} of the junction to be

$$J_{D-J} = \frac{\rho_{(S)}}{\rho_{(N)}}\frac{B_{c2}}{\mu_0\lambda_{(S)}\kappa}\hat{\psi}_\infty^2\left(\frac{B}{B_{c2}}\right)^{1/2}\left(\frac{2B}{B_{c2}}\frac{d^2}{\xi_{(S)}^2}+\frac{1}{\gamma}\right)^{1/2}F^2 \times \exp\left(-\frac{B\gamma}{B_{c2}}\frac{d^2}{\xi_{(S)}^2}\right). \quad (41)$$

4. Computational results

4.1. General considerations

The critical currents of various Josephson-junctions were calculated using TDGL theory and a transport current measurement approach equivalent to a standard four-terminal resistive measurement. The geometry of the SNS J-Js system is shown in figure 1. The external applied field had a gradient in the y-direction to provide a current travelling in the x-direction. The current enters and leaves the system as normal current, and then becomes supercurrent some way inside the superconductor. The total length of superconductor was typically set to $70\xi_{(S)}$. The current was ramped upwards in a series of steps, and the voltage across the junction calculated and averaged over the second half of each step. The voltage was computed by integrating the electric field in the direction of current flow to within $4\lambda_{(S)}$ of the ends of the system, which allows sufficient space for the injected normal current to become supercurrent, and then summing over all y within the superconductor. Zero voltage was used to obtain the critical current density J_c. Figure 2 shows examples of the current-versus-voltage characteristics used to extract J_c which show a sharp transition at low voltages which then broadens as seen experimentally [18]. Because of the normalized units used in this computational, data are shown in terms of H_{c2}. The experimental data shown in section 4.2 are shown in terms of B_{c2} where $B_{c2} = \mu_0 H_{c2}$. We are ultimately interested in equilibrium properties, where the time-dependent terms ultimately tend to zero so $\zeta' = \frac{\pi^4}{14\zeta(3)}$ was set to 1 in (2) to reduce computational expense which, consistent with work in the literature, does not affect the results [19, 20]. In wide thin junctions with high J_c values, the value of J_c for the junction as a whole is lowered as the current is excluded from the central region of the junction by the Meissner effect [21]. The importance of self-field limiting can be determined from

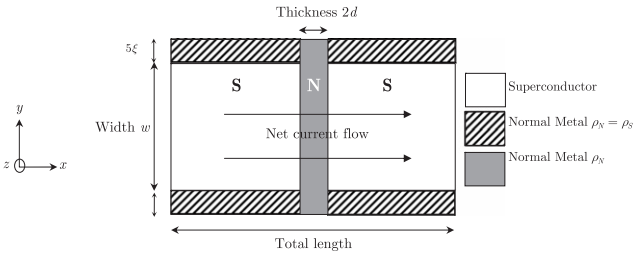

Figure 1. Diagram of an SNS Josephson-junction. The essential components are two superconducting slabs with a normal metal barrier between them.

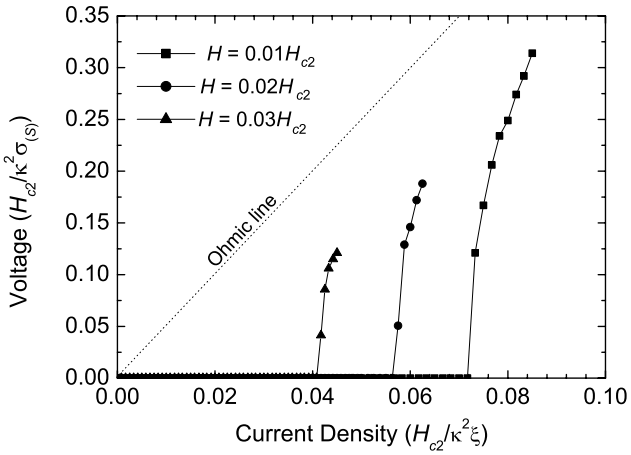

Figure 2. Computed V–I traces for a $30\xi_{(S)}$ wide, $0.5\xi_{(S)}$ thick junction with $\rho_{(N)} = 10\rho_{(S)}$.

the Josephson penetration depth [21] $\lambda_J = \sqrt{\frac{\hbar}{4eJ_c\mu_0(d+\lambda)}}$. We have confirmed computationally that for widths up to $10\xi_{(S)}$, $J_c(H=0) = J_{D-J}$, and that self-field effects only start to become important in zero field for a $30\xi_{(S)}$-wide junction when the junction thickness is below one coherence length.

4.2. Zero field computational data

Figure 3 shows J_c computed as a function of the junction thickness d, junction resistivity $\rho_{(N)}$ and κ for $\hat{\alpha}/\hat{\beta} = 1$ and $\hat{\alpha}/\hat{\beta} = 0$ where we have assumed $\frac{\rho_{(S)}}{\rho_{(N)}} = \frac{\xi^2_{(S)}}{\xi^2_{(DN)}}$. Making these substitutions into (20) with $\hat{\alpha}/\hat{\beta} = 1$ gives the normalized current density across the junction in zero field to be

$$\hat{J}_{D-J} = 2\sqrt{\frac{\rho_{(S)}}{\rho_{(N)}}}\left\{\sqrt{\frac{\rho_{(S)}}{2\rho_{(N)}}+1} - \sqrt{\frac{\rho_{(S)}}{2\rho_{(N)}}}\right\}^2 \times \exp\left(-2\hat{d}\sqrt{\frac{\rho_{(N)}}{\rho_{(S)}}}\right) \quad (42)$$

while (33) for $\hat{\alpha}/\hat{\beta} = 0$ gives

$$\hat{J}_{D-J} = \frac{\pi^2}{2}\left(\frac{\rho_{(S)}}{\rho_{(N)}}\right)^2\left(\hat{d} + \sqrt{\frac{2\rho_{(S)}}{\rho_{(N)}}\left(1+\sqrt{\frac{\rho_{(S)}}{\rho_{(N)}}}\right)}\right)^{-3}. \quad (43)$$

The thickness dependences of J_c for the SNS junctions obtained computationally are in almost exact accordance with (42) and (43) respectively. For both $\hat{\alpha}/\hat{\beta} = 0$ and $\hat{\alpha}/\hat{\beta} = 1$, $\hat{J}_{D-J}$ for a single SNS junction is κ-independent.

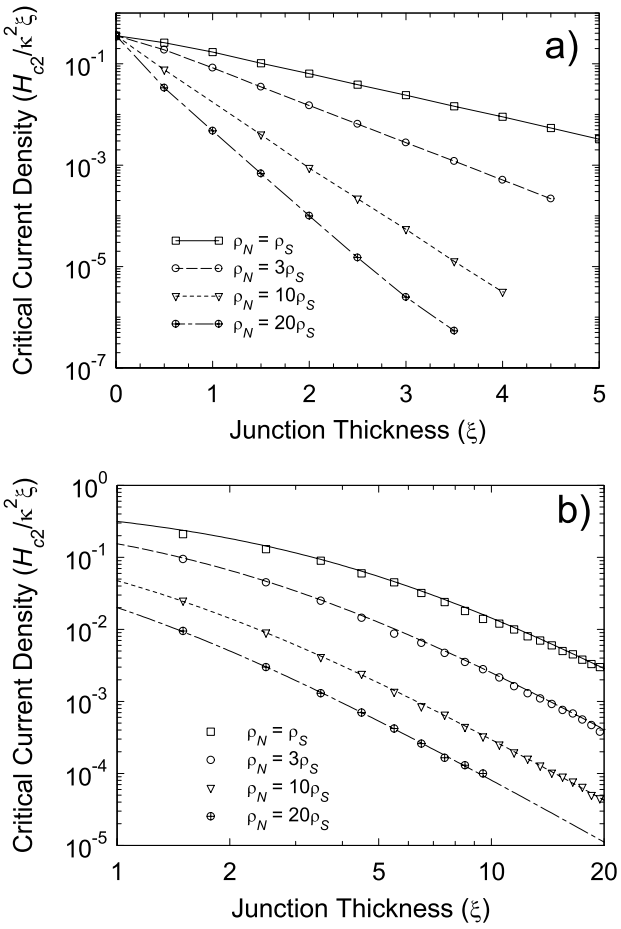

Figure 3. J_c values computed for a single $5\xi_{(S)}$ wide SNS junction with various junction resistivities for (a) $\hat{\alpha}/\hat{\beta} = 1$ and (b) $\hat{\alpha}/\hat{\beta} = 0$. The computational data (data points) correspond closely with the analytic results (42) and (43) respectively (lines).

4.3. Field dependence of J_c

In low fields, the superconducting blocks on either side of the junction are in the Meissner state and the critical current density leads to the familiar sinc function [22, 23]

$$J_c = \frac{J_c(B=0)\hbar}{2ew(d+\lambda)B_{app}}\left|\sin\frac{2ew(d+\lambda)B_{app}}{\hbar}\right| \quad (44)$$

where w is the width of the junction. We have confirmed using TDGL computation: for wider junctions, or junctions with a higher zero field J_c, the self-field resulting from the current flow becomes important; in the extreme limit, the self-field contribution causes the Fraunhofer sinc dependence to be replaced by a linear decrease of J_c with B, resulting from the confinement of the current to the edges.

When B is high enough that the superconductors on either side of the junction enter the mixed state, the standard textbook low field flux integration method is no longer valid [22]. Figure 4 shows the field dependences for $30\xi_{(S)}$-wide junction of varying thicknesses. These data are computationally expensive, particularly at low current density, so in order to find sufficient data points close to B_{c2} we have compromised on noise. For these wide junctions, individual nodes are not discernible in the field dependences of J_c. The J_c data in figure 4 have been fitted and the approximate form is

$$J_c(B) \approx J_{D-J}(B=0)\frac{\xi^2_{(S)}}{\sqrt{2}w(d+\xi_{(S)})}\frac{B_{c2}}{B}\left(1-\frac{B}{B_{c2}}\right). \quad (45)$$

This expression corresponds well with (44) where the oscillating term for these wide junctions has been averaged to $1/\sqrt{2}$, there is an additional $(1-\frac{B}{B_{c2}})$ factor which comes from the field dependence of $|\psi|^2$ and as is commonly assumed from physical arguments [24], the effective junction half-thickness has changed from $(d+\lambda)$ to $(d+\xi_{(S)})$. It can be noted that in figure 4 the computed values of J_c for fields above $0.6B_{c2}$ (for $d = 1.5\xi_{(S)}$) or $0.2B_{c2}$ (for $d = 3.5\xi_{(S)}$) are less than those predicted by (45). This is because J_{D-J} is decreased further by the presence of the field following an exponential field dependence [16] consistent with (41). The additional low-J_c line in figure 4(a) for $d = 3.5\xi_{(S)}$ is found by replacing the zero field J_{D-J} with the high field J_c given by (41) with the effective half-thickness of the junction set to $d+\xi_{(S)}$. Finally in figure 4(b), we show data for an SNS junction with an insulating boundary condition at the edges

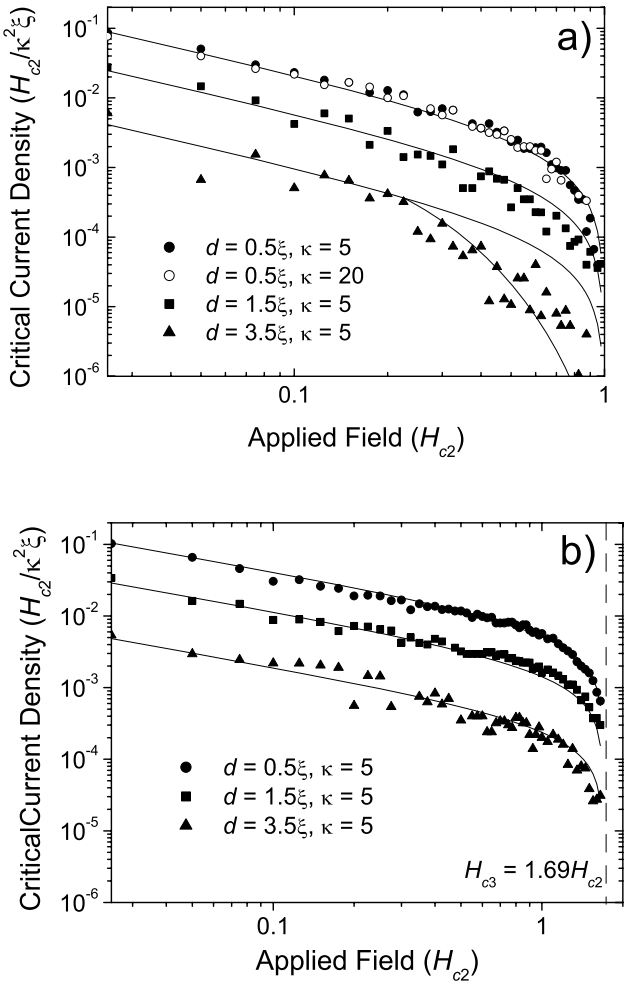

Figure 4. Field dependence of J_c up to H_{c2} for $30\xi_{(S)}$-wide $\rho_{(N)} = 3\rho_{(S)}$, $\alpha_N = 0$ junctions of various thicknesses in a $\kappa = 5$ superconductor coated with (a) $\rho_{(N)} = \rho_{(S)}$ metal and (b) insulator.

and fitted by the expression

$$J_c(B) \approx J_{D-J}(B=0)\frac{\xi^2_{(S)}}{2w(d+\xi_{(S)})}\left(\frac{1.69B_{c2}}{B}\right)^{0.66} \times \left(1-\frac{B}{1.69B_{c2}}\right)^{0.66}. \quad (46)$$

In the junction with insulating edges, current travels preferentially along the edges due to the superconducting surface sheath—this means the current through the junction is also dominated by the edges which, via the Fourier transform, changes the exponent from 1 to 0.66. B_{c2} is also replaced by $B_{c3} = 1.69B_{c2}$.

5. Comparison with experimental data on an SNS junction

In figure 5, the current density through a PbBi–Cd–PbBi SNS junction is shown from Hsaing and Finnemore's (HF) work [18]. There are two important features of these J_c data: (i) the strong temperature dependence of J_c in zero field (between ∼0.3 T_c (PbBi) and ∼0.7 T_c (PbBi), the critical current density changes by about four orders of magnitude) which we attribute to the decay of the order parameter in the normal metal characterized in equation (20) and (ii) the exponential magnetic field dependence which we attribute to the decay of the order parameter in magnetic fields as described in equation (41). We combine equations (20) and (41) together with (45) to account for the role of the phase of the order parameter, to provide a general equation for J_c given by:

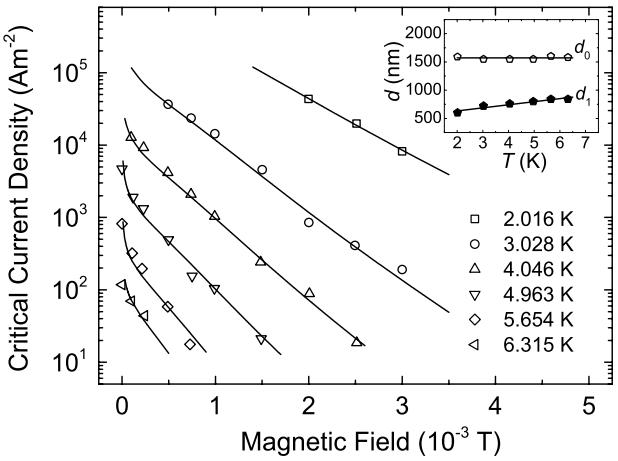

Figure 5. A fit to the experimental data from Hsiang and Finnemore for the critical current density through an PbBi–Cd–PbBi SNS junction as a function of temperature and magnetic field. The solid lines are obtained using equation (47) with two free parameters d_0 (nm) and d_1 (nm) which are the effective half-thicknesses of the normal barrier in zero field and in-field respectively.

$$J_c \approx \frac{\rho_{(S)}}{\sqrt{2}\rho_{(N)}}\frac{B_{c2}}{\mu_0\lambda_{(S)}\kappa}\frac{\xi^2_{(S)}}{w(d_1+\xi_{(S)})} \times \exp\left(-\frac{2d_0}{|\xi_{(DN)}|}\right)\left(\frac{B_{c2}}{B}\right)^{\frac{1}{2}}\left(\frac{2B}{B_{c2}}\frac{d_2^2}{\xi^2_{(S)}}+\frac{1}{\gamma}\right)^{\frac{1}{2}} \times F^2\left(1-\frac{B}{B_{c2}}\right)\exp\left(-\frac{B\gamma}{B_{c2}}\frac{d_2^2}{\xi^2_{(S)}}\right) \quad (47)$$

where we have distinguished the effective half-thickness of the normal layer associated with the decay of the order parameter in zero field (d_0), the phase of the order parameter (d_1) and the decay of the order parameter in high field (d_2). We have used the materials properties parameters listed in the HF paper [18] as follows: T_{cS}(PbBi) = 7.2 K, T_{cN}(Cd) = 0.52 K, $\rho_{(S)}/\rho_{(N)} = 10$, $J_c = I_c/A$ where the area of the junction, A, is 1.1×10^{-6} m^2 and the width of the junction, w, is 2.5×10^{-4} m. The PbBi was alloyed with Bi at 1–2% and the superconducting properties known to be similar to Pb [25]—the Ginzburg–Landau parameter for the superconductor, $\kappa = \lambda_{(S)}/\xi_{(S)}$ was taken to be 1 and $B_{c2}(T)$, was fixed using the WHH relation $B_{c2}(T) = B_{c2}(0)(1-t^{1.5})$, where $t = T/T_c$ is the reduced temperature [26–28] and $B_{c2}(0) = 80$ mT [25, 29]. For the normal metal decay length, $\xi_{(DN)}$, we used equation (11) and the relation that defines the

coherence length for a material whether above or below its critical temperature $m|\alpha| = \hbar^2/2\xi^2$ [30], so that:

$$|\xi_{(DN)}| = |\xi_{(N)}(T_{cS})| \left(\frac{T_{cS} - T_{cN}}{T - T_{cN}}\right)^{\frac{1}{2}}. \quad (48)$$

Although this work considers temperatures above $T_{cN}(\text{Cd}) = 0.52$ K when the Cd is non-superconducting, we can use the known superconducting properties of Cd to find an approximate value for $|\xi_{(N)}(T_{cS})|$. Using the values given for Cd [18] for the diffusivity, $D_N = 0.15$ m^2 s^{-1} and the Fermi velocity, $v_F = 7.7 \times 10^5$, the dirty limit expression from microscopic theory for the coherence length (i.e. $\xi_{(N)Dirty}(T_{cS}) = (\pi\hbar D/8k_B(T_{cS} - T_{cN}))^{\frac{1}{2}}$) and the clean limit expression (i.e. $\xi_{(N)Clean}(T_{cS}) = \hbar v_F/1.76\pi k_B T_{cN}^{0.5}(T_{cS} - T_{cN})^{0.5}$) we find values of 260 nm and 570 μm for the dirty and clean limits respectively [22]. Using Pippard's approach [31] (i.e. $\xi_{(N)}(T_{cS}) = ((\xi_{(N)Clean}(T_{cS}))^{-1} + (\xi_{(N)Dirty}(T_{cS}))^{-1})^{-1}$), we calculate $\xi_{(N)}(T_{cS})$ to be about 180 nm. Cd and Pb were chosen for these experiments in part because the solubility of Pb in Cd is negligible and hence the chemical properties change abruptly at the PbBi–Cd interface. The theory used in this paper applies to thick junctions where there is a relatively abrupt change in electronic properties at the interface between the PbBi and the Cd (equivalent to the requirement that for example, the electron scattering length, l, in the normal layer is much smaller than the half-thickness of the barrier) and $d_0 \approx d_1 \approx d_2$. However this thick limit assumption does not accurately apply to the PbBi–Cd–PbBi SNS junction considered here. Given that d_1 and d_2 both characterize the effective half-thickness of the normal layer in-field, we have made the assumption they are equal (i.e. d_1). Hence the solid lines in figure 5 are a best fit to the J_c data using equation (47) with two free parameters which are shown in the inset of figure 5 and have been allowed to be temperature dependent—the effective half-thicknesses of the normal barrier in zero field d_0 (nm) and in-field d_1 (nm) respectively.

The parameter d_0 is ~1.57 μm and almost temperature independent. It can be compared to the nominal or chemical, d_{Chem}, half-thickness for the Cd layer of 1.7 μm [32][1]. The agreement is within the uncertainties in the values and temperature dependences of the materials properties of the Cd. Nevertheless we also note that the effective thickness of the normal layer in zero field may be expected to be smaller than the chemical half-thickness, because in accordance with the uncertainty principle, the superconducting state may remain established a BCS coherence length inside the Cd (i.e. $d_0 = d_{Chem} - \xi_{BCS}$ where $\xi_{BCS}(\text{PbBi}) = 76$ nm [18]). The temperature dependence of the parameter d_1 (nm) is given by $d_1 = 526 + 54T$ where the temperature T is in kelvin. In the normal state, at temperatures above T_c(Pb–Bi) (i.e. 7.2–10 K where normal state measurements were made), we find that d_1 is 0.9–1 μm which is significantly smaller than d_{Chem}. Given that the electron scattering length for l(Cd), is about 600 nm (although note the resistivity of Cd in these junctions is uncertain to a factor two), we suggest the difference between the theoretical and experimental values of d_1 is due to the superelectrons first equilibrating a distance l(Cd) inside the Cd layer (i.e. $d_1 = d_{Chem} - l(\text{Cd})$) in-field. This explanation attributes the increase in d_1 to the decrease in l(Cd) with increasing temperature.

[1] There is a typographical error in the caption of figure 5 in Hsiang and Finnemore's paper. The thickness of the Cd layer is 3.4 μm. This correction can be deduced from the other data in the HF paper and has previously been identified in the paper by Dobrosavljevic-Grujic and Radovic [32].

6. Concluding comments and future work

The critical current density (J_c) through a technological high-J_c superconductor in high magnetic fields is controlled by the inclusions and microstructure of the material that hold fluxons stationary to keep the resistance zero [7, 33, 34] and described using scaling laws. We have long known that although characterizing grain boundary pinning using just the size of the grains is useful for describing similar superconducting materials with different grain sizes [35], it is very simplistic. Visualization of solutions to the TDGL equations for polycrystalline materials has shown that fluxons cross the superconductor by flowing along the grain boundaries [36] and demonstrate that local grain boundary properties must be important. Scaling laws are typically written in terms of a volume pinning force (F_p) which for grain boundary pinning in low temperature superconductors is of the form [5, 6, 35]:

$$F_p = J_c \times B = \frac{\alpha}{G} B_{c2}^n \left(\frac{B}{B_{c2}}\right)^p \left(1 - \frac{B}{B_{c2}}\right)^q \quad (49)$$

where B is the applied magnetic field, B_{c2} is the upper critical field, α, n, p and q are constants and G is the grain size. No local grain boundary properties are included. For polycrystalline A15 material, Chevrel-phase superconductors and MgB_2, p is approximately 0.5 and q is approximately 2 [5, 6]. If we assume that in high J_c superconductors, the De Gennes exponential term is not important, the exponential and $(1 - \frac{B}{B_{c2}})$ terms determine the field dependence in high fields. For Nb_3Sn, $d_1/\xi \sim 2$ which is equivalent to $q \approx 2$ in (49) [37, 38]. In low fields (47) leads to $J_c \propto B^{-0.5}$ which is equivalent to $p = 0.5$ in (49). The temperature dependence of F_p from (47) is equivalent to an n-value in (49) of ~2–2.5 as observed experimentally for Nb_3Sn. Hence, the field and temperature dependences in (47) are similar to the Kramer dependence which is widely found experimentally in polycrystalline LTS materials [6, 37, 38]—although it has long been known (since the elastic constants of the flux line lattice were calculated in the extreme high field limit) that the derivation used by Kramer is not valid [39]. The $1/w$ term in (47) is equivalent to the $1/G$ term in (49) and shows that although scaling laws describe the increase in J_c with increase in density of grain boundaries found experimentally [35], these increases in J_c may also be described using the junction model presented here [35]. Although we have not explicitly considered high temperature superconductors, the exponential field dependence for J_c is observed in many polycrystalline HTS materials consistent with thick normal grain boundaries [40–42]. These observations provide an

expectation that (47) can describe J_c in both LTS and HTS polycrystalline superconductors which is the subject of our future work [38].

Acknowledgments

We acknowledge the important and long-standing support of EPSRC. The authors acknowledge many useful discussions with Prapaiwan Sunwong who helped produce figure 5.

References

[1] Cardwell D and Ginley D 2003 *Handbook of Superconducting Materials* (Bristol: Institute of Physics Publishing)
[2] De Gennes P G 1989 *Superconductivity of Metals and Alloys* (Redwood City, CA: Addison Wesley)
[3] Hilgenkamp H and Mannhart J 2002 Grain boundaries in high-T_c superconductors *Rev. Mod. Phys.* **74** 485–549
[4] Sarrao J L 2006 *Basic Research Needs for Superconductivity: Report of the Basic Energy Sciences Workshop on Superconductivity* http://science.energy.gov/~/media/bes/pdf/reports/files/sc_rpt.pdf
[5] Dew-Hughes D 1974 Flux pinning mechanisms in type II superconductors *Phil. Mag.* **30** 293–305
[6] Kramer E 1973 Scaling laws for flux pinning in hard superconductors *J. Appl. Phys.* **44** 1360
[7] Ginzburg V L and Landau L D 1950 On the theory of superconductivity *Zh. Eksp. Teor. Fiz.* **20** 1064–82
[8] Brandt E H 1998 Superconductor disks and cylinders in an axial magnetic field. I. Flux penetration and magnetization curves *Phys. Rev.* B **58** 6506–22
[9] Schmid A 1966 A time dependent Ginzburg–Landau equation and its application to the problem of resistivity in the mixed state *Phys. Kondens. Mater.* **5** 302–17
[10] Hu C-R and Thompson R S 1972 Dynamic structure of vortices in superconductors, $H \ll H_{c2}$ *Phys. Rev.* B **6** 110–20
[11] Gor'kov L P 1960 Theory of superconducting alloys in a strong magnetic field near the critical temperature *Sov. Phys.—JETP* **10** 998–1004
[12] Usadel K D 1970 Generalized diffusion equation for superconducting alloys *Phys. Rev. Lett.* **25** 507–9
[13] Biagi K R, Kogan V G and Clem J R 1985 Perpendicular upper critical field of superconducting–normal-metal multilayers *Phys. Rev.* B **32** 7165–72
[14] Ivanov Z G, Kuprianov M Y, Likharev K K, Meriakri S V and Snigirev O V 1981 Boundary conditions for the Eilenberger and Usadel equations and properties of 'dirty' SNS sandwiches *Sov. J. Low Temp. Phys.* **7** 274–81
[15] Likharev K K 1979 Superconducting weak links *Rev. Mod. Phys.* **51** 102–59
[16] Dobrosavljevic-Grujic L and Radovic Z 1993 Critical currents in superconductor-normal metal-superconductor junctions *Supercond. Sci. Technol.* **6** 537–41
[17] Hurault J P 1966 Surface nucleation in a superconductor coated with a normal metal *Phys. Lett.* **20** 587–8
[18] Hsiang T Y and Finnemore D K 1980 Superconducting critical currents for thick, clean superconductor-normal-metal-superconductor junctions *Phys. Rev.* B **22** 154–63
[19] Gor'kov L P and Eliashberg G M 1968 Generalization of the Ginzburg–Landau equations for non-stationary problems in the case of alloys with paramagnetic impurities *Sov. Phys.—JETP* **27** 328–34
[20] Vodolazov D Y 2000 Effect of surface defects on the first field for vortex entry in type-II superconductors *Phys. Rev.* B **62** 8691–4
[21] Ferrell R A and Prange R E 1963 Self-field limiting of Josephson tunneling of superconducting electron pairs *Phys. Rev. Lett.* **10** 479
[22] Tinkham M 1996 *Introduction to Superconductivity* 2nd edn (Singapore: McGraw-Hill Book)
[23] Poole C P, Farach H A and Creswick R J 1995 *Superconductivity* (San Diego, CA: Academic)
[24] Nikulov A V and Remisov Y D 1991 The critical current of the Josephson junction with boundaries in the mixed state: application to HTSC polycrystalline materials *Supercond. Sci. Technol.* **3** 312–7
[25] Evetts J E and Wade J M A 1970 Superconducting properties and the phase diagrams of the Pb–Bi and Pb–In alloy systems *J. Phys. Chem. Solids* **31** 973–82
[26] Werthamer N R, Helfand E and Hohenberg P C 1966 Temperature and purity dependence of the superconducting critical field, H_{c2}. III. Electron spin and spin–orbit effects *Phys. Rev.* **147** 295–302
[27] Cheggour N and Hampshire D P 2002 The unified strain and temperature scaling law for the pinning force density of bronze-route Nb_3Sn wires in high magnetic fields *Cryogenics* **42** 299–309
[28] Godeke A, Jewell M C, Golubov A A, Ten Haken B and Larbalestier D C 2003 Inconsistencies between extrapolated and actual critical fields in Nb_3Sn wires as demonstrated by direct measurements of H_{c2}, H^* and T_c *Supercond. Sci. Technol.* **16** 1019–25
[29] Ashcroft N W and Mermin N D 1976 *Solid State Physics* (PA, USA: Sanders College Publishing)
[30] Tilley D R and Tilley J 1990 *Microscopic Theory of Superconductivity, in Superfluidity and Superconductivity* (Bristol: Institute of Physics Publishing) pp 119–22
[31] Orlando T P, McNiff E J, Foner S and Beasley M R 1979 Critical fields, Pauli paramagnetic limiting, and material parameters of Nb_3Sn and V_3Si *Phys. Rev.* B **19** 4545–61
[32] Dobrosavljevic-Grujic L and Radovic Z 1991 *Physica* C **185–189** 2313–4
[33] Josephson B D 1965 Supercurrents through barriers *Adv. Phys.* **14** 419–50
[34] Taylor D M J and Hampshire D P 2005 The scaling law for the strain dependence of the critical current density in Nb_3Sn superconducting wires *Supercond. Sci. Technol.* **18** S241–52
[35] Schauer W and Schelb W 1981 Improvement of Nb_3Sn high field critical current by a two-stage reaction *IEEE Trans. Magn.* **17** 374–7
[36] Carty G and Hampshire D P 2008 Visualising the mechanism that determines the critical current density in polycrystalline superconductors using time-dependent Ginzburg–Landau theory *Phys. Rev.* B **77** 172501
[37] Hampshire D P 1998 A barrier to increasing the critical current density of bulk untextured polycrystalline superconductors in high magnetic fields *Physica* C **296** 153–66
[38] Sunwong P, Higgins J S, Tsui Y, Raine M J and Hampshire D P 2012 The critical current density in polycrystalline HTS and LTS superconductors in high magnetic fields *Supercond. Sci. Technol.* submitted
[39] Hampshire D P, Jones H and Mitchell E W J 1985 An in-depth characterisation of $(NbTa)_3Sn$ filamentary superconductor *IEEE Trans. Magn.* **21** 289–92
[40] Lelay L, Friend C M, Maruyama T, Osamura K and Hampshire D P 1994 Evidence that pair breaking at the grain boundaries of $Bi_2Sr_2Ca_2Cu_3O_x$ tapes determines the critical current density above 10 K in high magnetic fields *J. Phys.: Condens. Matter* **6** 10053–66
[41] Senoussi S, Ousséna M, Collin G and Campbell I A 1988 Exponential H and T decay of the critical current density in $YBa_2Cu_3O_{7-\Delta}$ single crystals *Phys. Rev.* B **37** 9792–5
[42] Hampshire D P and Chan S-W 1992 The critical current density in high fields in epitaxial thin films of $YBa_2Cu_3O_7$: flux pinning and pair-breaking *J. Appl. Phys.* **72** 4220–6